Journal of Magnetic Resonance Open 16–17 (2023) 100104

Contents lists available at ScienceDirect

Journal of Magnetic Resonance Open

journal homepage: www.sciencedirect.com/journal/journal-of-magnetic-resonance-open

Research article

Low perturbation limit decoherence analyzed by scaling the Double Quantum Hamiltonian

C.M. Sánchez, H.M. Pastawski, A.K. Chattah *

Facultad de Matemática, Astronomía, Física y Computación - Universidad Nacional de Córdoba, 5000 Córdoba, Argentina
Instituto de Física Enrique Gaviola (CONICET-UNC), 5000 Córdoba, Argentina

ARTICLE INFO

Keywords:
Loschmidt echo
Scaling
Decoherence
Spin systems
Double Quantum

ABSTRACT

By varying the magnitude of the effective interaction between spins in relation to the perturbations, we study the decoherence behavior in a connected proton system. Making use of the Magnus expansion, we introduce a NMR pulse sequence that generates an average Hamiltonian with Double Quantum terms multiplied by a scaling factor, δ, with the possibility to take positive and negative values. The performance of the pulse sequence for different values of the scaling factors was validated in polycrystalline adamantane, by observing the evolution of the polarization. A time reversal procedure, accessible through the change of sign in the controlled Hamiltonian, was necessary to observe multiple quantum coherences. The spin counting develops a characteristic growth in two species of clusters for the scaled time. The influence of the scaling factor on the reversibility was observed through the behavior of the Loschmidt echoes, which decayed faster as the scaling factor increases. From the analysis of dynamics and its reversibility, we extracted characteristic times for the spin diffusion, T_2^δ and the intrinsic decoherence decay, T_3^δ for each scaling factor δ, and perturbation time scale, T_Σ. Observing the dependence of reversibility vs. perturbation rates, both normalized with the spin diffusion rate, we find that in the limit of low perturbations, T_2^δ/T_3^δ deviates from the linear dependence on T_2^δ/T_Σ that corresponds to strong perturbation. The asymptotic value $T_2/T_3 \approx 0.15$ as T_2^δ/T_Σ vanishes, gives evidence that the main source of irreversibility is the *intrinsic decoherence* associated to the chaotic many-body dynamics of the system.

1. Introduction

In 1950 the revolutionary observation of the *spin echo* by Erwin Hahn [1] manifested the time reversal of the precession of each *individual* spin. This required a radio-frequency (r.f.) pulse to switch the Zeeman Hamiltonian, $\mathcal{H}_Z$, into $-\mathcal{H}_Z$. Thus, the echo decay in time scale T_2 quantified the amount at which the spins interaction with each other limits such reversal. About two decades later, a new variant was able to achieve a goal sought since the times of Boltzmann and Loschmidt [2,3]: the time reversal of a complex many-body dynamics. The implemented procedure profits from the fact that in the quantum realm of multiple spins, dipolar dynamics occurs under an effective truncated dipolar Hamiltonian, $\mathcal{H}$, in the laboratory frame, whose sign changes into $-\frac{1}{2}\mathcal{H}$, in a rotating frame defined by a persistent resonant irradiation field. As consequence the original polarization, whose decay after a time t is assigned to multi-spin interactions, could be recovered in the form of a revival at $2t$ that deserved the name of *magic echo* (ME) [4–6]. Related time-reversal procedures were later implemented with great success to measure the coherences between different multi-spin projections denoted as *Multiple Quantum Coherences* (MQC) [7–9], which quantify the scrambling of the information originally localized in a individual spin. Nevertheless, a great mystery remained unsolved: Why the strength of the ME decays with a time scale smaller than the estimations resulting from the truncation terms and errors of the few pulses involved?. This mystery became even deeper when a time reversal of the spin diffusion dynamics, in the laboratory frame, of a localized polarization was achieved in the form of *polarization echoes* (PE) by Richard Ernst and collaborators [10], confronted similar limitations. These experiments were able to clarify the *local* nature of the information recovered as polarization after the reversal of the "spin diffusion" process. This fed a long term quest to address the issue of spin diffusion and emergent irreversibility [11–16]. At Córdoba, our team coined the term *Loschmidt echoes* (LE) to refer to *all the time reversal procedures* that could result from changing the sign of the effective Hamiltonian [17,18]. This failure of time reversal hints at a connection [16,19,20], within the quantum realm, with the controversy between Boltzmann and Loschmidt. We were inspired by

* Corresponding author at: Facultad de Matemática, Astronomía, Física y Computación - Universidad Nacional de Córdoba, 5000 Córdoba, Argentina.
E-mail address: karina.chattah@unc.edu.ar (A.K. Chattah).

https://doi.org/10.1016/j.jmro.2023.100104
Received 26 August 2022; Received in revised form 1 March 2023; Accepted 7 March 2023
Available online 10 March 2023

the *stosszahlansatz* idea of Boltzmann that the elastic collisions between particles in a gas would be irreversible "in practice". Also in a quantum system the diffusion constant, and other irreversibility magnitudes, depends only on the collision time scale, and not much on the precision with which those collisions are described [21]. Indeed, the natural chaotic instability of the many-body dynamics is quantified by the Lyapunov exponents, i.e. a property of the Hamiltonian not of the environment. Our approach requires the observation of the Loschmidt Echo, the signal recovered after forward and backward dynamics, under $\mathcal{H}$ and $-\mathcal{H}+\Sigma$, where its decay is produced by the influence of a small non-inverted term, the perturbation Σ. A semi-classical calculation shows that in a *high energy limit*, the exponential dynamical Lyapunov instability produces an exponential decay of the Loschmidt Echo for any small, though finite, Σ, as expected for a classical chaotic system [17,22,23]. This recovers the quantum–classical limit. While the discrete spectrum of a finite number of quantum spins prevents from applying this concept, the actual experiments are done in a crystal at room temperature. This ensures the thermodynamic limit of infinitely many-spins far from the ground state and a perturbation dynamics is progressively shrunk. This is the requirement for our "*Central Hypothesis of Irreversibility*" (CHI) which states that the memory of the initial conditions fades away in a time-scale T_3, which is mainly defined by the dynamics that one is able to revert, i.e. by T_2. That is, even when all the experimental errors and other departures from ideality could become negligible (*i.e.* $T_2/T_\Sigma \to 0$), the dynamics would remain irreversible with a time-scale T_3 which is intrinsically tied to the scrambling time of the specific Hamiltonian involved [24,25], i.e. to T_2. Thus, a number of experimental strategies had to be devised to implement the thermodynamic limit [26,27] in which the ratio T_2/T_Σ between the time scale characteristic of the Hamiltonian and the time scale of the perturbation and errors, could be swept towards the smallest possible values.

In the last decade we decided to start a program to test the Central Hypothesis of Irreversibility with experiments that could change the effective dipolar Hamiltonian with a scale factor δ while keeping the error terms roughly constant. This program was initiated by tilting the polarization at different angles around the magic direction, followed by an off-resonance irradiation [28,29]. Thus, both $\mathcal{H}$ and $-\mathcal{H}$ could be scaled down symmetrically. This was effective to study the growth of the MQC but it was not efficient to compare the time scales of time-reversal procedure, as the precision of the tilting angle was too critical. This limitation was overcame by a Floquet effective Hamiltonian engineered with the Magnus expansion. Through appropriate pulse sequences we implemented a *multi-pulse scaled dipolar interaction* (MPSDI) [30]. In this case, the ratio between scrambling time and actual irreversibility could be reduced until it reached a universal limit $T_2/T_3 \approx 1/7$. The same limiting value was latter re-obtained by using a strategy with completely different sources of errors: non symmetrical time reversal procedures consisting on a concatenation of a dynamics under off-resonance irradiation [31] with a MPSDI dynamic with adapted times. This provided enough variability on the forward a backward dynamics to confirm the limiting T_2/T_3 ratio for LE of the magic type.

In the meanwhile, the LE time reversal techniques acquired great momentum from an unexpected venue, that of Quantum Cosmology [32]. This came in the form of *Out of Time Order Correlations* (OTOCs), a family of mathematical objects that are particular cases of a LE [33,34]. The OTOCs were introduced by Susskind, Maldacena and co-authors as quantifiers of the degree of scrambling of quantum information as it evolves through the Hilbert space. This many-body quantum chaos context should occur in the extreme conditions around a black hole [35–37]. Such extreme quantum chaos regime, that occurs in the Sachdev–Ye–Kitaev (SYM) model, is required to establish a connection between a quantum fields theory and the Einstein theory of gravity within an idealized Maldacena's conjecture [33]. More generally, the OTOCs also allow to assess the complexity of a quantum circuits and quantum information [38]. This triggered an immense number of works in different related fields that led to great theoretical and experimental progress which is too extensive to be summarized here [34,39–42]. Within the field of NMR, these result a tool to quantify many-body localization, spin counting or to achieve dynamical decoupling [43–49]. However, it is central to our discussion to notice that, in the OTOCs, the *time reversibility* is given for granted. It is just a *tool* to assess the scrambling of the information, i.e. the complexity gained through forward dynamics [38]. Thus they are in full equivalence to the MQC in NMR, where time reversal is necessary to monitor the appearance of multi-spin correlations. However, while in MQC, weak perturbations degrade the signal, they *do not* affect the ratio between the various orders of coherences excited. These works did not attempt to address the mystery of the signal loss in LE/OTOC experiments. In contrast, our search seeks to use the LE to address the CHI and the emergence of a perturbation independent regime for the decoherence.

In the present work, we implement the thermodynamic limit for a LE dynamics that has not been addressed before, the *scaled double quantum* (SDQ) Hamiltonian. With this purpose we engineer the dipolar interaction through a multi-pulse sequence that we present here for the first time. Our effective Hamiltonian, can be used to evaluate the degree of scrambling in the Hilbert space, by estimating the number of correlated spins through a corresponding MQC/OTOC protocol. Our results confirm previous findings that a Double Quantum (DQ) Hamiltonian yields a ballistic spreading in the real space that corresponds to an exponential scrambling in the Hilbert space. The analysis of the LE intensities are once more compatible with the CHI.

2. Engineering a Floquet Hamiltonian through the Magnus expansion

We consider a system composed by $N \approx 10^{23}$ interacting spins-1/2, the ^{1}H in poly-crystalline adamantane [50], in the presence of a strong magnetic field, $\mathbf{B}_0 = B_0\hat{z}$, at room temperature. In the rotating frame, the system Hamiltonian is $\mathcal{H}_\mathrm{S} = \mathcal{H}_\mathrm{Z}^z + \mathcal{H}_\mathrm{d}^{zz}$, where the first term is the Zeeman Hamiltonian $\mathcal{H}_\mathrm{Z}^z = -\sum_i \Delta\omega_i I_i^z$, usually neglected as adamantane presents almost chemically equivalent spins and the radio-frequency is set on-resonance. The second term corresponds to the secular part of the dipolar Hamiltonian with respect to the external magnetic field ($\hbar = 1$),

$$\mathcal{H}_\mathrm{d}^{zz} = \sum_{i<j} d_{ij}(3I_i^z I_j^z - \mathbf{I}_i \cdot \mathbf{I}_j), \tag{1}$$

where the dipolar coupling strengths d_{ij} decrease with the internuclear distance as r_{ij}^{-3}, and $\mathbf{I}_i = \sum_i I_i^\alpha$ are total i-spin operators and $\alpha = x, y, z$. The notation $\mathcal{H}_\mathrm{d}^{\alpha\alpha}$ defines the secular dipolar Hamiltonian in the quantization axis α.

The total Hamiltonian under the presence of a cyclic time dependent interaction is

$$\mathcal{H}_\mathrm{Total}(t) = \mathcal{H}_\mathrm{S} + \mathcal{H}_\mathrm{cyc}(t). \tag{2}$$

The first terms is the system Hamiltonian previously described, and the second term accounts for the time-dependent control Hamiltonian, given by the on-resonance r.f. field driving in NMR experiments. An effective Floquet propagator for the time dependent Hamiltonian, can be obtained through the principles of *Average Hamiltonian Theory* (AHT) [51]. Particularly, when the time-dependent interaction has a cycle time t_c, and for stroboscopic observations at multiples of t_c, the toggling (interaction representation) and rotating lab frames coincide. Therefore, the Floquet propagator after n cycles, can be written in a form of a single exponential by means of the Magnus expansion,

$$\mathcal{U}_\mathrm{S}(nt_c) = \exp\left\{-\mathrm{i}\, nt_c \sum_{i=0}^{\infty} \mathcal{H}^i\right\}, \tag{3}$$

where the zeroth (also called effective or average) and first terms of this series written in the toggling frame, $\mathcal{H}_\mathrm{S}^\mathrm{togg}(t) = \mathcal{U}_\mathrm{cyc}^\dagger(t)\mathcal{H}_\mathrm{S}\mathcal{U}_\mathrm{cyc}(t)$, are: [51–53]

$$\mathcal{H}^0 = \frac{1}{t_c}\int_0^{t_c} dt' \mathcal{H}_\mathrm{S}^\mathrm{togg}(t'),$$

$$\mathcal{H}^1 = \frac{-\mathrm{i}}{2t_c}\int_0^{t_c} dt'' \int_0^{t''} dt' \left[\mathcal{H}_{\mathrm{S}}^{\mathrm{togg}}(t''), \mathcal{H}_{\mathrm{S}}^{\mathrm{togg}}(t')\right]. \quad (4)$$

Baum, Munowitz, and Pines described, in their pioneer works [8,9], one of the first applications of the AHT to engineer a new Floquet dynamics through multi-pulse sequences, defining the double quantum Hamiltonian,

$$\mathcal{H}_{\mathrm{DQ}} = \frac{1}{3}(\mathcal{H}_{\mathrm{d}}^{yy} - \mathcal{H}_{\mathrm{d}}^{xx}) = -\tfrac{1}{2}\sum_{i<j} d_{ij}(I_i^+ I_j^+ + I_i^- I_j^-), \quad (5)$$

We describe here our pulse sequence that results in the double quantum Hamiltonian. It consists in radio frequency (r.f.) pulses $\pi/2$ applied in defined phases (X, Y and their opposites $\overline{X}$, $\overline{Y}$), separated by free evolution times specially designed to obtain the desired dynamic. The delays are defined by, $\Delta_1 = \frac{\tau}{2}$ and $\Delta_2 = 2\tau$, where τ is an experimental parameter that determines the cycle duration t_c. The pulse sequence, named DQ_F, can be schematized as an ordered series of delays and pulses, producing the $\mathcal{H}_{DQ}$ Hamiltonian (at zero order),

$$\begin{array}{ccccccccccc} \Delta_1 & -X- & \Delta_2 & -X- & 2\Delta_1 & -\overline{X}- & \Delta_2 & -\overline{X}- & \Delta_1 \\ \Delta_1 & -\overline{X}- & \Delta_2 & -\overline{X}- & 2\Delta_1 & -X- & \Delta_2 & -X- & \Delta_1 \end{array}$$

By assuming that the r.f. pulses are instantaneous, the toggling-frame Hamiltonian is piece-wise constant. During the subsequent evolution periods, the toggling Hamiltonian is considered as the rotated version of the dipolar one, aligned with the external magnetic field (i.e. the z-direction of the rotating frame). The following scheme shows, in three different lines, the duration of free evolution periods (first line), and corresponding Hamiltonian terms in that periods: the Zeeman term (second line), and the dipolar term (third line), both in the toggling frame,

$$\begin{array}{ccccccccc} \Delta_1 & \Delta_2 & 2\Delta_1 & \Delta_2 & 2\Delta_1 & \Delta_2 & 2\Delta_1 & \Delta_2 & \Delta_1 \\ \mathcal{H}_{\mathrm{Z}}^{z} & \mathcal{H}_{\mathrm{Z}}^{y} & \mathcal{H}_{\mathrm{Z}}^{-z} & \mathcal{H}_{\mathrm{Z}}^{y} & \mathcal{H}_{\mathrm{Z}}^{z} & \mathcal{H}_{\mathrm{Z}}^{-y} & \mathcal{H}_{\mathrm{Z}}^{-z} & \mathcal{H}_{\mathrm{Z}}^{-y} & \mathcal{H}_{\mathrm{Z}}^{z} \\ \mathcal{H}_{\mathrm{d}}^{zz} & \mathcal{H}_{\mathrm{d}}^{yy} & \mathcal{H}_{\mathrm{d}}^{zz} & \mathcal{H}_{\mathrm{d}}^{yy} & \mathcal{H}_{\mathrm{d}}^{zz} & \mathcal{H}_{\mathrm{d}}^{yy} & \mathcal{H}_{\mathrm{d}}^{zz} & \mathcal{H}_{\mathrm{d}}^{yy} & \mathcal{H}_{\mathrm{d}}^{zz} \end{array}$$

The cycle time is the addition of all the evolution periods $t_c = 8\Delta_1 + 4\Delta_2 = 12\tau$. The zero order Hamiltonian is obtained as the weighted sum of the toggling-frame Hamiltonians at each time step [53]. This becomes in, $\mathcal{H}^0 t_c = 4\tau(\mathcal{H}_{\mathrm{d}}^{yy} - \mathcal{H}_{\mathrm{d}}^{xx})$. Then, for stroboscopic observation (multiples of cycle time), the average Hamiltonian has no Zeeman contribution, resulting in the DQ evolution (Eq. (5)).

Changing the phases of the pulses X and $\overline{X}$ by $\overline{Y}$ and Y respectively, it leads to the pulse sequence DQ_B, that produces the backward DQ evolution given by $-\mathcal{H}_{DQ}$. Double quantum dynamics represents a model evolution that motivated studies to understand MQC [7,54,55], OTOCs [56], decoherence and localization [57].

2.1. Zero order in the scaled double quantum dynamics

We introduce two variations of pulse sequences described above that produce the SDQ Hamiltonians of the form $\pm 2\delta\mathcal{H}_{DQ}$, with the factor δ. The basic unit to create the scaled DQ dynamics consists in 8 pulses (8P). The pulse sequence for the forward evolution, named DQ_F^δ, corresponds to the Hamiltonian with the + sign, while the one for the backward evolution, called DQ_B^δ corresponds to the - sign. The zero order term in the Magnus expansion (Eq. (4)), for each case is obtained in the same way than in the preceding section.

The time delays for the free evolution periods in the scaled pulse sequences are,

$$\Delta_1 = \frac{\tau}{2}(1+\delta) \qquad \Delta_2 = \tau(1-\delta)$$
$$\Delta_3 = 2\tau(1+2\delta) \qquad \Delta_4 = 2\tau(1-2\delta) \quad (6)$$

where δ defines the scaling of the Hamiltonian and τ is related to the cycle time t_c.

The basic block of 8 pulses for the scaled DQ forward evolution, DQ_F^δ(8P), is schematized as,

$$\begin{array}{cccccccccc} \Delta_1 & -X- & \Delta_3 & -\overline{X}- & \Delta_2 & -Y- & \Delta_4 & -Y- & \Delta_1 \\ \Delta_1 & -Y- & \Delta_4 & -\overline{Y}- & \Delta_2 & -\overline{X}- & \Delta_3 & -\overline{X}- & \Delta_1 \end{array} \quad (7)$$

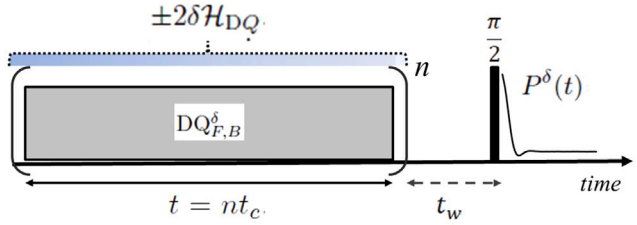

(a) Polarization evolution, $P^\delta(t)$, under the forward or backward Hamiltonian. The dynamics is obtained applying n times each DQ_F^δ (or DQ_B^δ) block, such that t is a multiple of the cycle time t_c. The waiting time t_w cancels unwanted ringing.

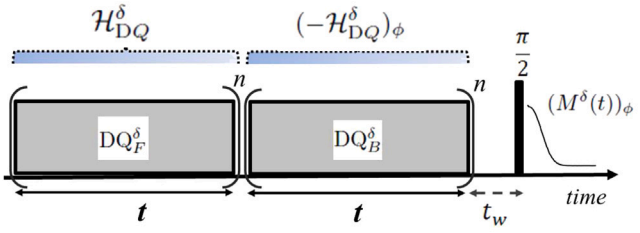

(b) The measurement of the magnitude $(M^\delta(t))_\phi$ requires a time-reversal procedure with same forward and backward times. The backward block involves a rotation around z axis with phase ϕ. The Loschmidt echo $M^\delta(t)$ corresponds to the signal with no rotation, $\phi = 0$.

Fig. 1. Experimental implementations to measure polarization, Loschmidt echoes and MQC, under the SDQ Hamiltonian.

For each free evolution time in this sequence the toggling frame Hamiltonians (Zeeman and dipolar terms) are,

$$\begin{array}{ccccccccc} \Delta_1 & \Delta_3 & \Delta_2 & \Delta_4 & 2\Delta_1 & \Delta_4 & \Delta_2 & \Delta_3 & \Delta_1 \\ \mathcal{H}_{\mathrm{Z}}^{z} & \mathcal{H}_{\mathrm{Z}}^{y} & \mathcal{H}_{\mathrm{Z}}^{z} & \mathcal{H}_{\mathrm{Z}}^{-x} & \mathcal{H}_{\mathrm{Z}}^{-z} & \mathcal{H}_{\mathrm{Z}}^{x} & \mathcal{H}_{\mathrm{Z}}^{-z} & \mathcal{H}_{\mathrm{Z}}^{-y} & \mathcal{H}_{\mathrm{Z}}^{z} \\ \mathcal{H}_{\mathrm{d}}^{zz} & \mathcal{H}_{\mathrm{d}}^{yy} & \mathcal{H}_{\mathrm{d}}^{zz} & \mathcal{H}_{\mathrm{d}}^{xx} & \mathcal{H}_{\mathrm{d}}^{zz} & \mathcal{H}_{\mathrm{d}}^{xx} & \mathcal{H}_{\mathrm{d}}^{zz} & \mathcal{H}_{\mathrm{d}}^{yy} & \mathcal{H}_{\mathrm{d}}^{zz} \end{array}$$

The cycle time is the addition of all delays appearing in (7), $t_c = 2(2\Delta_1 + \Delta_2 + \Delta_3 + \Delta_4) = 12\tau$. By using AHT, the zero order term satisfies $\mathcal{H}^0 t_c = 8\tau\delta(\mathcal{H}_{\mathrm{d}}^{yy} - \mathcal{H}_{\mathrm{d}}^{xx})$. Then, the DQ_F^δ sequence produces a scaled *forward* Hamiltonian of the form,

$$\mathcal{H}_{\mathrm{DQ}}^\delta = 2\delta\frac{(\mathcal{H}_{\mathrm{d}}^{yy} - \mathcal{H}_{\mathrm{d}}^{xx})}{3}$$

The same calculation can be performed for DQ_B^δ, corresponding to the *backward* pulse sequence

$$\begin{array}{ccccccccccc} \Delta_1 & -\overline{Y}- & \Delta_3 & -Y- & \Delta_2 & -\overline{X}- & \Delta_4 & -\overline{X}- & \Delta_1 \\ \Delta_1 & -\overline{X}- & \Delta_4 & -X- & \Delta_2 & -Y- & \Delta_3 & -Y- & \Delta_1 \end{array}$$

resulting in the scaled backward zero order Hamiltonian

$$-\mathcal{H}_{\mathrm{DQ}}^\delta = 2\delta\frac{(\mathcal{H}_{\mathrm{d}}^{xx} - \mathcal{H}_{\mathrm{d}}^{yy})}{3}$$

Both forward and backward pulse sequences $\mathrm{DQ}_{F,B}^\delta$ were designed to have the same number of pulses and same cycle time as the $\mathrm{DQ}_{F,B}$. The parameter τ is a variable time selected to enforce a safe minimum separation between r.f. pulses. As it can be extracted from Eqs. (6), the admitted values for δ correspond to the interval $[0, 1/2)$. Experimental implementation requires greater restrictions that limit the accessible values even more, because of a minimum waiting time between pulses is required.

Experimentally, the composition of two 8P blocks in an anti-symmetric 16P sequence showed a better performance (see experimental Appendix). These 16P forward and backward versions have the advantage of canceling odd terms in the Magnus expansion (Eq. (4)).

The zero order Hamiltonian remains the same than in the 8P case, and the cycle time is twice as long, ($t_c = 24\tau$), then

$$\pm\mathcal{H}^{\delta}_{\mathrm{DQ}} t_c = \pm 16\tau\delta(\mathcal{H}^{yy}_{\mathrm{d}} - \mathcal{H}^{xx}_{\mathrm{d}})$$

resulting,

$$\mathcal{H}^{\delta}_{DQ} = 2\delta\mathcal{H}_{\mathrm{DQ}} \quad \text{and} \quad -\mathcal{H}^{\delta}_{DQ} = -2\delta\mathcal{H}_{DQ}. \tag{8}$$

3. Spreading of the initial excitation

The Floquet evolution of the thermal initial state I^z under the influence of $\pm\mathcal{H}_{DQ}$ or $\pm\mathcal{H}^{\delta}_{DQ}$, can be obtained as the magnetization measured in the pulse sequence depicted in Fig. 1(a). We call $P(t)$ to the measurement obtained for the evolution under Double Quantum Hamiltonian without scaling and propagator $\mathcal{U}(t) = \exp\left(-\mathrm{i}\mathcal{H}_{DQ}t\right)$. The measurement of the signal with scaled evolution is expressed as,

$$P^{\delta}(t) = \mathrm{Tr}[\mathcal{U}^{\delta\dagger}(t) I^z \mathcal{U}^{\delta}(t) I^z]/\mathrm{Tr}[I^z I^z] \tag{9}$$

where the propagator is $\mathcal{U}^{\delta}(t) = \exp\left(-\mathrm{i}2\delta\mathcal{H}_{DQ}t\right)$. From the thermal initial state the system evolves under the average Hamiltonian, $\pm\mathcal{H}_{DQ}$ or $\pm\mathcal{H}^{\delta}_{DQ}$, during an experimental time that is multiple of the cycle time, $t = nt_c$. Fig. 2 shows the evolution of the polarization $P(t)$ and the various $P^{\delta}(t)$, obtained by using the 16 pulse sequences DQ_F and DQ^{δ}_F, where the cycle time is $t_c = 24\tau$. Fig. 2(a) displays the polarization as a function of the experimental time $t = n24\tau$, where τ was varied in the range 5–10 μs and the integer n was selected such as $t \lesssim 3$ ms.

The signal obtained in the case of DQ (that is, $P(t)$, diamonds in Fig. 2(a)) displays the faster evolution with a marked oscillation followed by an attenuation to zero. $P^{\delta}(t)$ reproduces this behavior but slowed down by the scale factor δ. In the extreme value $\delta = 0$, the polarization $P^{\delta=0}(t)$ shows no oscillation as expected, but the signal decay is showing up the errors due to the experimental implementation and the importance of the higher order terms in the Magnus expansion. This information is used to normalize the data, filtering the dynamics of uncontrolled factors. Fig. 2(b) displays $P(t)/P^{\delta=0}(t)$ and $P^{\delta}(t)/P^{\delta=0}(t)$ as a function of a scaled time $t_s = 2\delta t$.

Given the limitations of the accessible experimental times which are multiples of 24τ, the fastest $P(t)$ curve for the DQ sequence loses the information of the initial decay, presenting the first data at 120 μs, showed by an arrow in Fig. 2(b). The measurements with SDQ dynamics allow to access to those short times information, otherwise inaccessible. The reconstruction of the original DQ curve with the data obtained from scaled dynamics was carried out with the information of different scale factors in different time ranges. For short times (less than 120 μs) the $\delta = 0.1$ curve (red dots) is the one that provides more detailed information (closer points), departing from the expected behavior as time grows. This separation is due to the accumulation of experimental errors produced by the repetition of a large number of cycles (n), necessary to achieve the equivalent time of the original dynamics, $t_s = 2(0.1)nt_c$. At longer times, the curves for $\delta = 0.2$ or 0.35 show better agreement to follow the oscillation of the original DQ dynamic. This provides the information on the range of validity of the best scale factors at different evolution times.

The backward sequences DQ_B and DQ^{δ}_B were also implemented. The resulting curves of $P^{-\delta}(t)$ (not shown) overlap with the corresponding ones in Fig. 2(a), which guarantees the possibility to implement a reliable temporal reversion of the dynamics and the observation of Loschmidt echoes and MQC.

3.1. Obtaining the spreading time T_2

Abragam's book [58] proposes, without mathematical proof, a function with good agreement for the fitting of the experimental FID in a solid system,

$$P(t) = \mathrm{sinc}(wt) \times \exp[-(ht)^2/2], \tag{10}$$

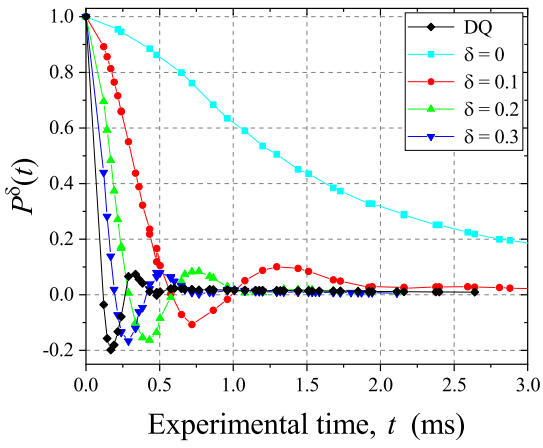

(a) Polarization as a function of experimental time.

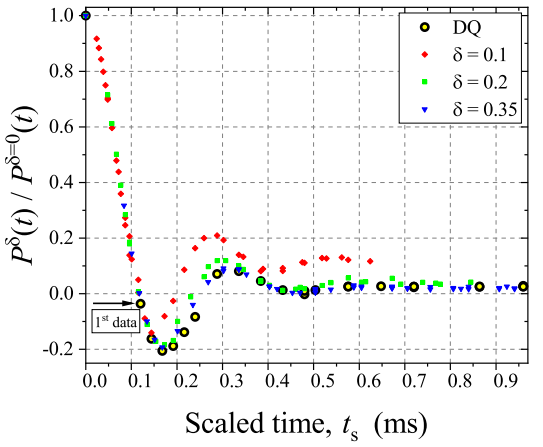

(b) Normalized polarization as a function of scaled time. The arrow shows the first data of the original DQ dynamics at 0.12 ms. The evolution of P^{δ} for different values of δ was used to complete the original curve at different range times.

Fig. 2. Polarization dynamics under original $\mathcal{H}_{DQ}$, and scaled $\mathcal{H}^{\delta}_{DQ}$ for different values of δ. The noise level of this measurement is lower than the dispersion of the data for scaled times greater than 0.8 ms, where the signal oscillates around zero.

which captures both the decay and the damped oscillation arising from the unitary dynamics. The parameters w and h participate in the series expansion of the function $P(t)$, and they are related with the second and fourth moments of the distribution. The second moment $M_2 = h^2 + w^2/3$, is related with the *spreading* time scale T_2 as $M_2 = (1/T_2)^2$.

Fig. 3 shows the calculated values for $1/T^{\delta}_2$ as a function of the different factors 2δ, in the same manner done for the dipolar case in our previous works [30,31]. These T^{δ}_2 values will be used in Section 6 to evaluate the region where the perturbations are less relevant compared to the intensity of the dynamics.

The linear behavior ensures that the scaling is working properly. The parameters of the fitting are: intercept = (0.88 ± 0.09) ms^{-1}; slope = (14.3 ± 0.2) ms^{-1}. Ideally, $\delta = 0$ should not show dynamics or decay. Experimentally, we observed a decay due to the different sources of uncontrolled errors, see Fig. 2(a). Then for $\delta = 0$, the intercept is not strictly at the origin, but reflects the limit of our control of the pulse sequence. Hints of this, can be seen in the big error bar for $\delta = 0.05$ in Fig. 3.

The fitting of the linear behavior observed in Fig. 3 for the scaled Hamiltonian ($2\delta < 1$), when evaluated for $2\delta = 1$, reproduces the value

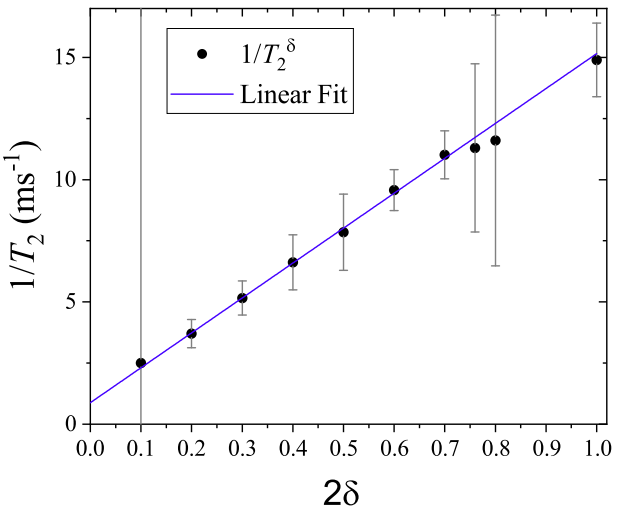

Fig. 3. Plot of $1/T_2^{\delta}$ vs 2δ.Values of T_2^{δ} were obtained by fitting the Abragam function to $P(t)$ or $P^{\delta}(t)$.

obtained from the measurement with original, not scaled DQ sequence, $1/T_2 = (15 \pm 1)$ ms^{-1}.

The errors bars associated to the data reflect greater problems in the extreme values, $\delta = 0.05$ and $\delta > 0.35$. In the first case, as the scale factor is small, the perturbation is more important than the dynamic that we intend to observe. At the other extreme, the problems come from the implementation of the sequence, which requires pulses that are too close together.

4. Time reversal and the Loschmidt echoes

The possibility to implement time reversal procedure, i.e. to have forward dynamics followed by a backward one, is fundamental for the measurement of LEs and MQCs, as shown in Fig. 1(b). The figure displays a forward block of scaled dynamics ($\mathcal{H}^{\delta}_{DQ}$) of duration t followed by another block of the same duration with reversed dynamics rotated around z by a phase shift ϕ, $(-\mathcal{H}^{\delta}_{DQ})_{\phi}$.

The experimental procedure to obtain the Loschmidt echo for a state that has spread a time t corresponds to no rotation, that is a phase $\phi = 0$. The signal acquired after the read-out pulse is the survival of the initial state,

$$M^{\delta}(t) = \mathrm{Tr}[\mathcal{U}'^{\delta\dagger}(t)\mathcal{U}'^{(-\delta)\dagger}(t)I^z\mathcal{U}'^{(-\delta)}(t)\mathcal{U}'^{\delta}(t)I^z]/\mathrm{Tr}[I^zI^z] \tag{11}$$

In the ideal case that backward evolution goes to the exact initial state the Loschmidt echo is identically 1, $M^{\delta}(t) \equiv 1$. Intrinsic irreversibility and non controlled factors lead the decay of the LE signal. Indeed, we have defined in previous works a *decoherence* characteristic time T_3, at which the LE decays to one half [30,31,43]. In the present case, each T_3^{δ}, is obtained as, $M^{\delta}(T_3^{\delta}) = 1/2$, .

Fig. 4(a) displays the LE measurements under the SDQ Hamiltonian for different δ factors as a function of the experimental time. Also it shows the behavior obtained with the original double quantum pulse sequence. It is notable how as the many-body interactions grows (δ values increase) the irreversibility is stronger, affecting the decay of the signal. Fig. 4(b) displays the normalized LE, obtained by dividing $M^{\delta}(t)$ by the reference $M^{\delta=0}(t)$. This normalization extract from the data the loss of information produced by errors in the time-reversal implementation (higher order terms in Magnus expansion, non-ideality in pulses, etc.), which are similar for every δ value. The $\delta = 0$ curve captures this influence, and not the one due to DQ dynamics. Then, the decay of $M^{\delta=0}(t)$, characterizes a *perturbation* time T_{Σ}, obtained from $M^{\delta=0}(T_{\Sigma}) = 1/2$. To verify that the remaining decay (that is, what survives normalization) is associated with the scaled Hamiltonian

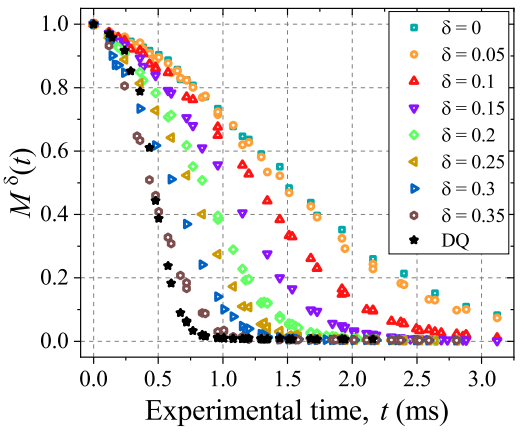

(a) Loschmidt echoes as a function of experimental time. The decay rate of the echoes increases with δ. The curve for $\delta = 0$ (no DQ dynamics) is used for normalization.

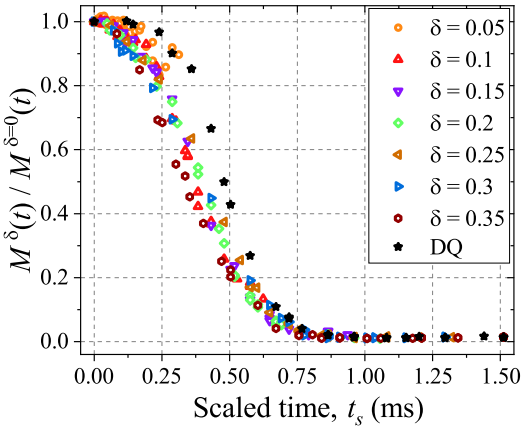

(b) Normalized Loschmidt echoes as a function of scaled time. This representation of the echoes shows an overlap in a single behavior for the scaled dynamics.

Fig. 4. Loschmidt echoes decay under $\mathcal{H}_{DQ}$ and $\mathcal{H}^{\delta}_{DQ}$ for various different δ factors. The noise level is lower than the dispersion of the data for scaled times greater than 1.0 ms, where the signal no longer retrieves relevant information.

dynamics, a plot of the normalized echoes as a function of the scaled (or proper) time of the dynamic $t_s = 2\delta t$, is shown. In this figure it is possible to observe how all the curves of the different LEs, $M^{\delta}(t)/M^{\delta=0}(t)$, collapse into a single one. Despite this collapse in a single behavior, characteristic of the SDQ, it is noticeable a departure from the curve obtained with the original DQ sequence, which survives better at short times (stars in Fig. 4(b)). This difference can be explained by the Magnus expansion terms of higher orders, which behave different between these sequences. Currently, some new experiments are being carried out to modify the pulse sequence, assessing further manifestation of the effect of the higher order terms in the Magnus expansion. Preliminary results show differences in the form of the LE decay, achieving a better agreement with the corresponding to the original DQ.

5. Spin counting

The difference in the total spin projection between two coupled multi-spin states is defined as the coherence number n. The dynamic consequence of the application of the Hamiltonian is to extend the network of connections which produces a redistribution of the longitudinal

magnetization in different coherence orders, which are not directly observable.

In order to measure the spectrum of coherence orders, we implemented the experimental scheme of Fig. 1(b). The rotation ϕ applied in the second block around the axis of quantization, z, is used to encode the coherence orders, as explained in Refs. [7,43,54]. The signal acquired after the reading pulse, $(M^{\delta}(t))_{\phi}$, is a function of the evolution time t and the phase ϕ, and can be expressed as the sum of each coherence order intensity marked by $n\phi$,

$$(M^{\delta}(t))_{\phi} = \sum_{n} e^{i\phi n}(S^{\delta}(t))_{n} \tag{12}$$

The rotation angle ϕ is a multiple of $\frac{2\pi}{2^L}$, which determines the maximum observable coherence order. The full collection of $(M^{\delta}(t))_{\phi}$ for the 2^L different values of ϕ provides the necessary information to extract the coherence intensities, $(S^{\delta}(t))_{n}$, through Fourier transformation in Eq. (12). As the state to be observed becomes increasingly complex, the value of L is adapted experimentally, to decode the higher coherence orders developed.

Note that the signal corresponding to the measurement with $\phi = 0$ is the Loschmidt echo, and is equivalent to the addition of all the coherence order intensities at a given time, i.e., $(M^{\delta}(t))_{\phi=0} = \sum_{n}(S^{\delta}(t))_{n}$.

For each time, the coherence order spectrum gives information on the number of correlated spins. To extract a representative value, N, for each state, the Baum model fits a Gaussian to $(S^{\delta}(t))_{n}$, leading to the spin counting [9,59,60].

We have shown the existence of superposition states with the contribution of two clusters of different sizes, in the case of Double Quantum evolution in adamantane [54]. This clusters are denoted as N_1 and N_2, the small one and a large one respectively. Therefore the best fitting to the spectra for each time t, consists of a sum of two Gaussians,

$$(S^{\delta})_{n} = \sum_{i=1}^{2} \frac{2A_i^{\delta}}{\sqrt{N_i^{\delta}\pi}} e^{(-n^2/N_i^{\delta})} \tag{13}$$

where the amplitudes A_i^{δ} correspond to the fraction of each cluster, while N_i^{δ} is the cluster size, representing the complexity of the correlated state.

Fig. 5 displays the evolution of both clusters size, $N_{1,2}^{\delta}$, for different values of the scaled factor δ and for the original, not scaled, DQ sequence. It is noticeable the superposition of each cluster in a single global behavior for all the scale factors, since the data are plotted against scaled time, t_s. For scaled times $t_s > 0.2$ ms, the separation in two clusters is evident. In the figure we have added the points corresponding to the experiments with the extreme scale factor 0.41, to highlight the departure of the results from the global curve. This is due to the excessively demanding experimental implementation, with inter-pulse duration less than 1 μs. Therefore, we do not expect that these points represent adequate values, since we are not achieving with the sequence, the dynamics that we want to implement. Nevertheless, as occurs for the XY [61] and DQ [55] dynamics in 1D, our SDQ dynamics should be ballistic. This implies that a local excitation spreads linearly with time with a group velocity satisfying the Lieb–Robinson bound [62] . In our 3D systems, a whole sphere around the initial point remains entangled, which this implies σ correlated spins at the time unit τ. Thus, we fit the data of the second "cluster" to

$$N_2(t_s) \approxeq 1 + (\sigma - 1)(t_s/\tau)^3 \tag{14}$$

with $(\sigma - 1)/\tau^3 \approx 3000 \times \mathrm{ms}^{-3}$ that contains the detailed information on the crystal structure and the topology of the coupling network.

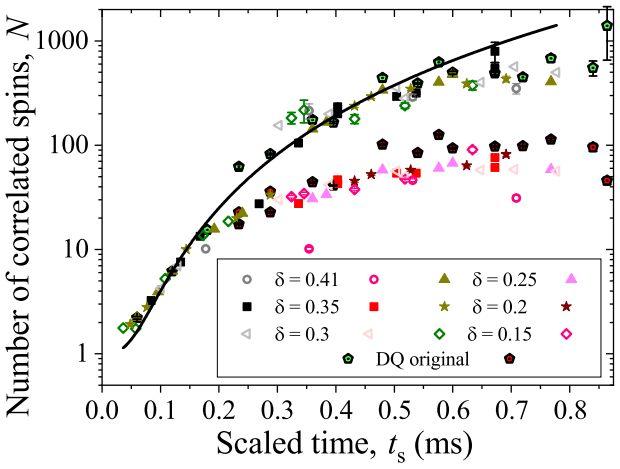

Fig. 5. Cluster size vs. t_s for $\mathcal{H}_{DQ}^{\delta}$ and different values of δ factors, plotted together with the cluster size evolution for the original $\mathcal{H}_{DQ}$. The separation in two clusters is observed for $t_s > 0.2$ ms, the small one N_1, and the large N_2, for all the Hamiltonians under study. Error bars are included, many of them are smaller than the size of the marker. The black line represents the ballistic dynamics of Eq. (14).

6. Dynamical irreversibility and decoherence

Previous experiments and results in our group have suggested that when time reversal is implemented in a complex quantum system the irreversibility time scale, in principle, is controlled by all the non-idealities Σ of the procedure. Such Σ could be interpreted as an energy uncertainty arising from truncation terms in the Magnus expansion, systematic pulse errors, or non-accounted terms in the Hamiltonian. In the experiments where the Hamiltonian can be scaled down, those non-idealities are captured by the LE decay time T_{Σ} observed when $H \equiv 0$. In spite of the fact that there are many cases where these non-idealities had been identified and substantially reduced, the reversibility time could not be extended beyond a time scale T_3, which we dubbed *intrinsic decoherence*. In fact, even having changed the system and/or the effective Hamiltonian, T_3 always seemed to be roughly proportional to T_2, the time scale of the reversed and controlled dynamics that scrambles the initial excitation [24,25,30].

In the Ref. [24] it was suggested that a way to quantify the relation between these time scales, can be achieved by displaying the experimental values of T_2/T_3 vs T_2/T_{Σ}. Then, for different Hamiltonians, the intrinsic value obtained as $T_2/T_{\Sigma} \to 0$, would correspond to the thermodynamics limit when the imperfections become less important compared to the dynamics. In Fig. 6 we show this plot for the SDQ dynamics, and the original DQ. Then, the decoherence rate $1/T_3^{\delta}$ versus the perturbation rate $1/T_{\Sigma}$, both normalized with the spreading rate $1/T_2^{\delta}$, are shown for different δ values. The times T_3^{δ} were extracted from the echoes, while T_2^{δ} are shown in Fig. 3. A key experimental observation, is that the cancellation of the Hamiltonian for $\delta = 0$ enables to measure $T_{\Sigma} = T_3^{\delta=0}$, that is the signal decay, resulting from the non-inverted terms in addition to experimental limitations, that is not "amplified" by the DQ dynamics.

Indeed, previous works dealing with scaled dipolar dynamics [30,31], allowed us to verify that in the range where the *perturbations* are important compared to the controlled dynamics, the values of T_2/T_3 gets close to T_2/T_{Σ} (represented by the diagonal straight line Fig. 6). In the opposite limit of low errors, we can appreciate the influence of multi-spin dynamics in the intrinsic T_3. Conceptually, this function was inspired by assuming that the LE still accounts for two Gaussian processes: a trivial one associated with the perturbation in absence of dynamics, and the other in which even a small perturbation acts through the dynamics and yields the constant A. The data manifests a departure from the trivial linear behavior giving a saturation of the

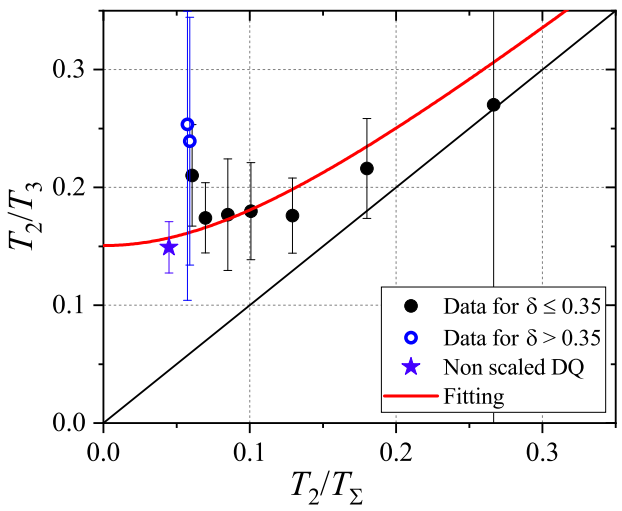

Fig. 6. Normalized decoherence rate T_2^δ/T_3^δ vs normalized perturbation rate T_2^δ/T_Σ, for various values of δ and the original DQ. The rate $1/T_2^\delta$ corresponds to the controlled dynamics imposed to the system and was used for normalization. The vertical axis measures the deviation of the controlled dynamics due to the intrinsic complexity of the system, while the horizontal axis is a measure of the experimental limitations. In the limit of vanishing perturbation, T_2/T_3 saturates to the value of 0.15. The diagonal is shown to follow the behavior for slow dynamics. The fitting function $y = \sqrt{A + x^2}$ with $A = 0.023 \pm 0.003$ is plotted in red. (For interpretation of the references to color in this figure legend, the reader is referred to the web version of this article.)

value of T_2/T_3, indicating the perturbation independent regime. The experimental data for scaled DQ dynamics show the same tendency of our previous results, see dots in Fig. 6. Indeed, we have verified, that the function that superimposes two Gaussian processes, $y = \sqrt{A + x^2}$ has the expected behavior in the two limits of high and low perturbation, showing an excellent agreement with a large set of experimental data in a T_2/T_3 vs T_2/T_Σ plots [30,31]. Although now the data set for the DQ scaled dynamics is smaller, we proceeded to fit the preceding function to the experimental points, as shown in Fig. 6, obtaining a good agreement with the behavior and yielding $A = 0.023 \pm 0.003$. The crossing with the vertical axis determines the asymptotic value $T_2/T_3 \approx \sqrt{A} = 0.15 \pm 0.01$.

The points corresponding to $\delta > 0.35$, shown with empty circles in Fig. 6, were not considered for the fitting. As explained before, they were measured in extreme experimental conditions. This fact was also observed in the big errors associated to T_2 in Fig. 3. It is remarkable that the point indicated with a star, corresponding to DQ without scaling, i.e. when the acting Hamiltonian is as perfect as possible, follows the global behavior. This confirms the emergence of an intrinsic decoherence in the limit of low disturbances.

The separation of data from the diagonal for fast dynamics (closer to the origin), gives evidence of a signal loss associated with the dynamics rather than the perturbations. Then, a decay of the Loschmidt echo more related to the dynamics imposed on the system, can be understood as an intrinsic decoherence associated with its complexity. This is notable in a regime of *perturbation independent decay* (PID) of the LE, achievable when the dynamics become fast and therefore the experimental errors are less significant.

7. Conclusions

We have introduced the time reversal of the SDQ dynamics to evaluate the influence of the perturbations on the reversibility. Varying the strength $1/T_2$ of the SDQ Hamiltonian while the time scale of the disturbances, T_Σ, remains roughly constant, we were able to swipe through their relative time scales, T_2/T_Σ, with their lowest values approaching the thermodynamic limit of infinitesimal perturbation.

Before turning into the qualitative implications of our results, we want to highlight some technical novelties of the present work: (i) We designed a completely new sequence, not found in previous literature, to scale the DQ Hamiltonian, (ii) The experimental section describes the optimization of the sequence and its implementation. In addition, we analyzed the measured data for forward and backward evolution, echoes, and the spin counting through multiple quantum coherences. The performance of the SDQ sequence was evaluated by comparing the dynamics generated with different factors δ with respect to the non scaled DQ. Regions of very good agreement were found, and conditions where the experimental implementation no longer works correctly were identified at the higher values of T_2/T_Σ, (iii) The forward dynamics with DQ for the short time regime has not been previously published. As we show, the original DQ dynamics is too fast to be observed at stroboscopic times, multiples of the sequence cycle. By slowing down the dynamics, the SDQ allowed to study the behavior at short times, not accessible with the original sequence,

It is noticeable that the number N of correlated spins under DQ evolution grows faster than in dipolar case [31], reaching around 1000 correlated spins for times ≈ 0.8 ms. This is consistent with a ballistic dynamics were N grows roughly as t^3 for all the implementations (scaled and non scaled DQ). This might be assimilated with a *butterfly effect* [42], in analogy with the behavior of classically chaotic systems, as it implies an exponential growth of the number of correlated (entangled) states in the Hilbert space. The present results contrast with the diffusive growth of $N \propto t^{3/2}$ we observed for transverse polarization under dipolar dynamics [30]. There, the secular term of the Hamiltonian conspires against the non-secular DQ dynamics by inducing a form of many-body localization [57]. Under a more detailed scrutiny of the fitting laws, it became clear that there are two representative sets of spins that could be identified as two clusters. The first, $N_1(t)$, reaches a finite size while a possible asymptotic values for the second, $N_2(t)$, could not be discriminated with certainty from the unbounded cubic growth because of experimental errors that dominate the long evolution times. In that sense our data do not contradict the findings of Alvarez and collaborators [57,63].

In general, we have repetitively attempted to split and isolate the consequences of different error sources. Some of these are: Experimental errors including rotations, higher-order terms of the effective Hamiltonian, non-idealities of the experimental system, and a number of further items. It took us about a decade to work out many of these details. Just to recall some of the most relevant ones: **(a)** We eliminated the quadrupolar nuclei, used by the Ernst group to speed up the experiments in their crystal, by growing pure crystals. Thus, we observed the mesoscopic echoes that were previously missed [14,61] and inspired the first implementation of a quantum channel [64], **(b)** We allowed the relaxation processes to become dominant over the Hamiltonian dynamics by decoupling the dipolar interaction [19] **(c)** We changed and improved the phase cycling to diminish errors. This allowed us to predict and detect heteronuclear coherences as high frequency oscillations in the polarization [14,16]. Further on, we showed that multi-nuclear coherence dynamics could undergo a Quantum Dynamical Phase Transition [65] **(d)** We used different magnetic fields and radio-frequencies power as well as different crystal orientations [20] to shrink the relevance of the truncation terms [19]. **(e)** We changed the topology of the spin–spin interaction by the spin-network in different forms, by diluting the active spin networks, and even consider finite spin systems in the form of liquid crystals [43,66]. However, as long as they are not too bold, they become inextricably entangled by the quantum dynamics as they do not commute with the Hamiltonian. Thus, as our chaotic system is evolving in time, we concluded that such an attempt necessarily would miss an emergent non-perturbative behavior. In summary, whatever we did to improve these early experiments and in the new ones, the irreversibility timescales could not be extended much further than that observed by Rhim, Pines and Waugh.

We thus set our present strategy, jointly devised with our missed collaborator Patricia Rebeca Levstein [24,28], seeking to use different "artillery" at hand to cancel out the many-body dynamics [19]. This would let the time scale T_Σ of the "errors/perturbations" to manifest itself experimentally. Only then, these "perturbative" processes is allowed to act over the excitation progressively scrambled by a Hamiltonian dynamics. It is this strategy what finally allows us to approach experimentally the "thermodynamic limit", in which a quantum dynamics of the large scale δ region is much stronger than the perturbation strength. In the other end, the range of small δ values, gives us the magnitude of non controlled errors, and provides a *crucial* time dependent normalization for the whole set of LE data. While the errors cannot be reduced, its relative importance is shrank by turning on the SDQ Hamiltonian strength until it reaches an *intrinsic irreversibility limit*. Indeed, this tentative conclusion is not obvious at all as it would involve a limiting case of quantum mechanics which has not yet been worked out theoretically. Besides, a numerical test of such thermodynamic limit is out of the reach of the classical computational capabilities [42,67,68] or even beyond the present quantum computers [69]. Quite on the opposite side, the *conservation of information* is often assumed, as Hawking and Susskind did, as a "minus-first law" of Nature [70] that confronts the information paradox [71,72]. In contrast, while our systems are not as much chaotic as the ideal SYK model [36], our experiments seem indicative of a broken time-reversal symmetry [73,74] which would be missed by a theory that could not account for the non-uniformity of the subtle thermodynamic limit [26, pp. 78] of $N \to \infty$ previous to make $\Sigma \to 0$ for the normalized Loschmidt echo observable.

In the present work we addressed, to the best of our possibilities, the condition $\Sigma \to 0$ of the thermodynamic limit for a local excitation evolving in a crystal ($N \approx 10^{23}$) under the double-quantum Hamiltonian by making $T_2/T_\Sigma \ll 0$. We found, in agreement with previous works, that once the quantum dynamics scrambling acquires a dominant role, i.e. as T_2 becomes much shorter than T_Σ, the dynamics amplifies the residual perturbation terms to the degree that it imposes $T_3 \approx 6.7T_2$, which is just a few times T_2. It is important to notice that direct decay due to perturbation could be roughly removed from the different Loschmidt echoes time dependence by normalizing the full curves with $M^{\delta=0}(t)$, the echo in absence of dynamics (Fig. 4 b). Thus, the observed decay of the different $M^{\delta}(t)/M^{\delta=0}(t)$ is mainly due to the Hamiltonian "amplification" of the residual terms in Σ. However, the full emergence of the irreversibility is best captured when presented in terms of the relative decay times of Fig. 6. In our previous work on the transverse excitation under the dipolar dynamics, the limiting decay remained the same for different pulse-sequence implementations, each of which involved different errors [27,31]. Here, also the same limit is obtained from the SDQ *and* the traditional DQ Hamiltonian. Thus, while one cannot issue an absolute statement, the present results, in conjunction with all the previous experiments, is definitely supportive of our CHI. This relays on the emergence [24,75] of a regime of *perturbation independent decay* of the coherence also dubbed *intrinsic decoherence* [17]. Notice again that we actually observe *irreversibility*. The term *decoherence* addresses the fact that the residual effects of non-idealities and perturbations can only manifest through the action of the fast Hamiltonian dynamics of our many-body system.

Data availability

Data will be made available on request.

Acknowledgments

We acknowledge the support of the grants from CONICET, SeCyT-UNC, and FoNCyT.

Declaration of competing interest

The authors declare that they have no known competing financial interests or personal relationships that could have appeared to influence the work reported in this paper.

Appendix. Experimental procedure

The experiments were performed in a Bruker Avance II spectrometer operating at 300 MHz Larmor frequency. The sample temperature was controlled along the experiments at 303 K. Besides, it was not observed appreciable heating effects produced by the continuous r.f. irradiation.

The pulse duration of $\pi/2$ was typically of $t_p = 2$ μs. The basic block of the scaled double quantum sequences DQ^{δ}_{F} and DQ^{δ}_{B} as well as the $\mathrm{DQ}_{F,B}$ is composed by 8 pulses (8P) separated by different lapses. Experimentally the anti-symmetric pulse sequences, composed by 16 pulses with opposite phases in the second train of 8 pulses, demonstrated better performance than the corresponding basic block.

Considering the finite duration of the pulses t_p the free evolution periods must be calculated as,

$$\Delta_1 = \frac{\tau}{2}(1+\delta) - t_p/2 \qquad \Delta_2 = \tau(1-\delta) - t_p$$
$$\Delta_3 = 2\tau(1+2\delta) - t_p \qquad \Delta_4 = 2\tau(1-2\delta) - t_p$$

The antisymmetric versions of the 16 pulses (16P) sequence, include free evolution periods and pulses in definite phases. For forward case the zero order of the average Hamiltonian is $\mathcal{H}^{\delta}_{\mathrm{DQ}} = 2\delta\mathcal{H}_{\mathrm{DQ}}$ and the schematic representation results, DQ^{δ}_{F} (16P)

$$\begin{array}{cccccccccc}
\Delta_1 & -X- & \Delta_3 & -\overline{X}- & \Delta_2 & -Y- & \Delta_4 & -Y- & \Delta_1 \\
\Delta_1 & -Y- & \Delta_4 & -\overline{Y}- & \Delta_2 & -\overline{X}- & \Delta_3 & -\overline{X}- & \Delta_1 \\
\Delta_1 & -X- & \Delta_3 & -X- & \Delta_2 & -Y- & \Delta_4 & -\overline{Y}- & \Delta_1 \\
\Delta_1 & -\overline{Y}- & \Delta_4 & -\overline{Y}- & \Delta_2 & -X- & \Delta_3 & -\overline{X}- & \Delta_1
\end{array}$$

The same can be done to obtain the Hamiltonian for the backward evolution with 16P sequences. The zero order Hamiltonian $-\mathcal{H}^{\delta}_{\mathrm{DQ}} = -2\delta\mathcal{H}_{\mathrm{DQ}}$ and the pulse sequence, DQ^{δ}_{B} (16P),

$$\begin{array}{cccccccccc}
\Delta_1 & -\overline{Y}- & \Delta_3 & -Y- & \Delta_2 & -\overline{X}- & \Delta_4 & -\overline{X}- & \Delta_1 \\
\Delta_1 & -\overline{X}- & \Delta_4 & -X- & \Delta_2 & -Y- & \Delta_3 & -Y- & \Delta_1 \\
\Delta_1 & -\overline{Y}- & \Delta_3 & -\overline{Y}- & \Delta_2 & -\overline{X}- & \Delta_4 & -X- & \Delta_1 \\
\Delta_1 & -X- & \Delta_4 & -X- & \Delta_2 & -\overline{Y}- & \Delta_3 & -Y- & \Delta_1
\end{array}$$

The cycle time is the same for forward and backward cases of 16P, $t_c = 8\Delta_1 + 4(\Delta_2+\Delta_3+\Delta_4) = 24\tau$, not depending on the pulse duration. The parameter τ is related directly to the inter-pulse duration. For each δ, τ was varied in the range 5 to 10 μ to reconstruct the main features of the magnetization evolution. Cycle time took values from 120 to 240 μs, while the experimental evolution time is a multiple of the cycle time, and was less than 3 ms in every implemented experiment. Due to experimental limitations, the inter-pulse duration were not smaller than 1 μs. This produces that for large values of δ only big values of τ are allowed experimentally, leading to dispersed points in a rapid dynamics.

The values of δ implemented were {0, 0.05, 0.1, 0.15, 0.2, 0.25, 0.3, 0.35, 0.4, 0.41}. Producing scaling factors 2δ multiplying the DQ Hamiltonian. The Δ_4 interpulse duration for $\delta = 0.41$ are ≈ 1 μs for the larger used values of τ so we could not go further, representing our experimental limit. On the other hand, enlarging the value of τ causes a loss of precision in the calculation of the average Hamiltonian.

Having the set up of DQ^{δ}_{F}, DQ^{δ}_{B}, sequences, we use these as unit blocks in experiments to obtain the evolution under a scaled double quantum Hamiltonian for the polarization, the Loschmidt echoes, and the multiple quantum coherences. That is schematized in Fig. 1. The Fig. 1(a) shows the implementation for the measurement of the polarization evolution, $P^{\delta}(t)$, under the forward or backward Hamiltonian. The Hamiltonian is obtained applying n times each DQ^{δ}_{F} (or DQ^{δ}_{B}) blocks, resulting in an evolution time $t = nt_c$. The waiting time

t_w previous to the final read-out pulse, cancels out unwanted ultra-fast multi-spin dynamics. The Fig. 1(b) displays the measurement of $(M^{\delta}(t))_{\phi}$ that involves a time-reversal procedure with same forward and backward times t. According to the values of δ and the evolution time t of the state to observe, the phases ϕ were implemented in steps of $2\pi/128$ or $2\pi/256$, decoding coherence orders up to $n = 64$ and $n = 128$ respectively.

References

[1] E. Hahn, Phys. Rev. 80 (1950) 580–594.
[2] T.S. Kuhn, Black-Body Theory and the Quantum Discontinuity, 1894-1912, University of Chicago Press, ISBN: 9780226458007, 1987.
[3] J.L. Lebowitz, Phys. Today 46 (9) (1993) 32.
[4] W.-K. Rhim, H. Kessemeier, Phys. Rev. B 3 (1971) 3655–3661.
[5] W.-K. Rhim, A. Pines, J.S. Waugh, Phys. Rev. Lett. 25 (1970) 218–220.
[6] W.-K. Rhim, A. Pines, J.S. Waugh, Phys. Rev. B 3 (1971) 684–696.
[7] J. Baum, M. Munowitz, A.N. Garroway, A. Pines, J. Chem. Phys. 83 (1985) 2015.
[8] M. Munowitz, A. Pines, Science 233 (1986) 525–531.
[9] J. Baum, A. Pines, J. Am. Chem. Soc. 108 (1986) 7447–7454.
[10] S. Zhang, B.H. Meier, R.R. Ernst, Phys. Rev. Lett. 69 (1992) 2149–2151.
[11] P.R. Levstein, H.M. Pastawski, R. Calvo, J. Phys.: Condens. Matter 3 (1991) 1877–1888.
[12] H.M. Pastawski, Phys. Rev. B 44 (1991) 6329.
[13] H.M. Pastawski, Phys. Rev. B 46 (1992) 4053–4070.
[14] H.M. Pastawski, P.R. Levstein, G. Usaj, 1995, pp. 4310–4313, 75.
[15] H.M. Pastawski, G. Usaj, Phys. Rev. B 57 (1998) 5017–5020.
[16] P.R. Levstein, G. Usaj, H.M. Pastawski, J. Chem. Phys. 108 (1998) 2718.
[17] R.A. Jalabert, H.M. Pastawski, Phys. Rev. Lett. 86 (2001) 2490–2493.
[18] A. Goussev, R.A. Jalabert, H.M. Pastawski, D.A. Wisniacki, Scholarpedia 7 (8) (2012) 11687.
[19] G. Usaj, H.M. Pastawski, P.R. Levstein, Mol. Phys. 95 (1998) 1229–1236.
[20] H. Pastawski, P. Levstein, G. Usaj, J. Raya, J. Hirschinger, Physica A 283 (2000) 166–170.
[21] R.B. Laughlin, Nuclear Phys. B Proc. Suppl. 2 (1987) 213–224.
[22] F.M. Cucchietti, H.M. Pastawski, R.A. Jalabert, Phys. Rev. B 70 (2004) 035311, (see Figs. 4, 5 and 6).
[23] G. Benenti, G. Casati, Phys. Rev. E 65 (2002) 066205.
[24] P.R. Zangara, H.M. Pastawski, Phys. Scr. 92 (2017) 033001.
[25] P.R. Zangara, D. Bendersky, P.R. Levstein, H.M. Pastawski, Phil. Trans. R. Soc. A 374 (2016) 20150163.
[26] A.L. Fetter, J.D. Walecka, Quantum Theory of Many-Particle Systems, McGraw-Hill, Boston, 1971.
[27] C.M. Sánchez, A.K. Chattah, K.X. Wei, L. Buljubasich, P. Cappellaro, H.M. Pastawski, Phys. Rev. Lett. 124 (2020) 030601.
[28] L. Buljubasich, C.M. Sánchez, A.D. Dente, P.R. Levstein, A.K. Chattah, H.M. Pastawski, J. Chem. Phys. 143 (2015) 164308.
[29] C.M. Sánchez, L. Buljubasich, H.M. Pastawski, A.K. Chattah, J. Magn. Reson. 281 (2017) 75–81.
[30] C.M. Sánchez, A.K. Chattah, K.X. Wei, L. Buljubasich, P. Cappellaro, H.M. Pastawski, Phys. Rev. Lett. 124 (2020) 030601.
[31] C.M. Sánchez, A.K. Chattah, H.M. Pastawski, Phys. Rev. A 105 (2022) 052232.
[32] R. Cowen, Nature 527 (2015) 290–293.
[33] A. Kitaev, 2017, in Brown Physics Colloquium, March 6, URL https://youtu.be/pFBAm7UCFHQ.
[34] M. Schleier-Smith, Nat. Phys. 13 (2017) 724–726.
[35] D.A. Roberts, D. Stanford, L. Susskind, J. High Energy Phys. 2015 (03) (2015) 051.
[36] J.M. Maldacena, S.H. Shenker, D. Stanford, J. High Energy Phys. (Online) 2016 (8) (2016) 106.
[37] J.M. Maldacena, Nat. Rev. Phys. 2 (3) (2020) 123–125.
[38] A.R. Brown, L. Susskind, Phys. Rev. D 97 (2018) 086015.
[39] R. Fan, P. Zhang, H. Shen, H. Zhai, Sci. Bull. 62 (2017) 707–711.
[40] R.J. Lewis-Swan, A. Safavi-Naini, J.J. Bollinger, A.M. Rey, Nature Commun. 10 (2019) 1581.
[41] X. Mi, P. Roushan, C. Quintana, S. Mandrà, J. Marshall, C. Neill, F. Arute, K. Arya, J. Atalaya, R. Babbush, et al., Science 374 (6574) (2021) 1479–1483.
[42] T. Zhou, B. Swingle, 2021, arXiv:2112.01562v1 [quant-ph].
[43] C.M. Sánchez, P.R. Levstein, L. Buljubasich, H.M. Pastawski, A.K. Chattah, Phil. Trans. R. Soc. A 374 (2016) 20150155.
[44] K.X. Wei, P. Peng, O. Shtanko, I. Marvian, S. Lloyd, C. Ramanathan, P. Cappellaro, Phys. Rev. Lett. 123 (2019) 090605.
[45] X. Nie, B.-B. Wei, X. Chen, Z. Zhang, X. Zhao, C. Qiu, Y. Tian, Y. Ji, T. Xin, D. Lu, J. Li, Phys. Rev. Lett. 124 (2020) 250601.
[46] M. Niknam, L.F. Santos, D.G. Cory, Phys. Rev. Res. 2 (2020) 013200.
[47] F. Lozano-Negro, P.R. Zangara, H.M. Pastawski, Chaos Solitons Fractals 150 (2021) 111175.
[48] F.D. Domínguez, G.A. Álvarez, Phys. Rev. A 104 (2021) 062406.
[49] M. Kuffer, A. Zwick, G.A. Álvarez, PRX Quantum 3 (2022) 020321.
[50] I. Schnell, H.W. Spiess, J. Magn. Reson. 151 (2001) 153–227.
[51] U. Haeberlen, High Resolution NMR in Solids, Academic Press, ISBN: 0-12-025561-8, 1976.
[52] C.P. Slichter, Principles of Magnetic Resonance, Springer-Verlag, Berlin; New York, 1990.
[53] R.R. Ernst, G. Bodenhausen, A. Wokaun, Principles of Nuclear Magnetic Resonance in One and Two Dimensions, Oxford Univ. Press, Oxford, 1987.
[54] C.M. Sánchez, R.H. Acosta, P.R. Levstein, H.M. Pastawski, A.K. Chattah, Phys. Rev. A 90 (2014) 042122.
[55] E. Rufeil-Fiori, C.M. Sánchez, F.Y. Oliva, H.M. Pastawski, P.R. Levstein, Phys. Rev. A 79 (2009) 032324–032329.
[56] H. Cho, T.D. Ladd, J. Baugh, D.G. Cory, C. Ramanathan, Phys. Rev. B 72 (2005) 054427.
[57] G.A. Álvarez, D. Suter, R. Kaiser, Science 349 (2015) 846–848.
[58] A. Abragam, Principles of Nuclear Magnetism, Reprinted, Oxford Univ. Press, 2007.
[59] M. Munowitz, A. Pines, in: S.A.R. I. Prigogine (Ed.), Principles and Applications of Multiple-Quantum NMR, John Wiley and Sons, Inc., 1987.
[60] M. Munowitz, A. Pines, M. Mehring, J. Chem. Phys. 86 (1987) 3172–3182.
[61] H.M. Pastawski, G. Usaj, P.R. Levstein, Chem. Phys. Lett. 261 (1996) 329–334.
[62] E.H. Lieb, D.W. Robinson, Comm. Math. Phys. 28 (1972) 251–257.
[63] G.A. Álvarez, D. Suter, Phys. Rev. Lett. 104 (2010) 230403.
[64] Z. Mádi, B. Brutscher, T. Schulte-Herbrüggen, R. Brüschweiler, R. Ernst, Chem. Phys. Lett. 268 (1997) 300–305.
[65] G.A. Álvarez, E.P. Danieli, P.R. Levstein, H.M. Pastawski, J. Chem. Phys. 124 (19) (2006) 194507.
[66] P.R. Levstein, A.K. Chattah, H.M. Pastawski, J. Raya, J. Hirschinger, J. Chem. Phys. 121 (2004) 7313–7319.
[67] A.D. Dente, C.S. Bederián, P.R. Zangara, H.M. Pastawski, GPU accelerated Trotter-Suzuki solver for quantum spin dynamics, 2013, arXiv, URL https://arxiv.org/abs/1305.0036.
[68] P.R. Zangara, D. Bendersky, H.M. Pastawski, Phys. Rev. A 91 (2015) 042112.
[69] B. Yan, N.A. Sinitsyn, Phys. Rev. Lett. 125 (2020) 040605.
[70] H.R. Brown, J. Uffink, Stud. Hist. Phil. Mod. Phys. 32 (4) (2001) 525–538.
[71] J. Horgan, Sci. Am. (2020) URL https://www.scientificamerican.com/article/will-the-universe-remember-us-after-were-gone/.
[72] Y. Nomura, Sci. Am. (2020) URL https://blogs.scientificamerican.com/observations/have-we-solved-the-black-hole-information-paradox/.
[73] P.W. Anderson, Science 177 (1972) 393–396.
[74] P.W. Anderson, Basic Notions of Condensed Matter Physics, Addison Wesley, Reading, Mass., 1984.
[75] S. Chibbaro, L. Rondoni, A. Vulpiani, Reductionism, Emergence and Levels of Reality, Springer, 2014.